SUPPLEMENTAL MATERIAL

Discovering precise temporal patterns in large-scale neural recordings through robust and interpretable time warping

Alex H. Williams[1,*,†], Ben Poole[9], Niru Maheswaranathan[9], Ashesh K. Dhawale[10,11], Tucker Fisher[1], Christopher D. Wilson[14], David H. Brann[10,11], Eric Trautmann[1], Stephen Ryu[5, 12], Roman Shusterman[13], Dmitry Rinberg[14,15], Bence P. Ölveczky[10,11], Krishna V. Shenoy[3,4,5,6,7,8], Surya Ganguli[2,3,4,5,6,7,9,*]

[1]Neuroscience Program, [2]Applied Physics Department, [3]Neurobiology Department, [4]Electrical Engineering Department, [5]Bioengineering Department, [6]Bio-X Program, [7]Wu Tsai Stanford Neurosciences Institute, [8]Howard Hughes Medical Institute
Stanford University, Stanford, CA 94305, USA.

[9] Google Brain, Google Inc.
Mountain View, CA 94043, USA.

[10]Department of Organismic and Evolutionary Biology, [11]Center for Brain Science
Harvard University, Cambridge, MA 02138, USA.

[12]Department of Neurosurgery
Palo Alto Medical Foundation, Palo Alto, CA 94301, USA.

[13]Institute of Neuroscience
University of Oregon, Eugene, OR 97403, USA.

[14]Neuroscience Institute
New York University School of Medicine, New York, NY 10016, USA. [15]Center for Neural Science
New York University, New York, NY 10016, USA.
[16]Center for Neural Science
New York University, New York, NY 10016, USA.

[*]Send correspondence to ahwillia@stanford.edu, sganguli@stanford.edu; [†]Lead Contact

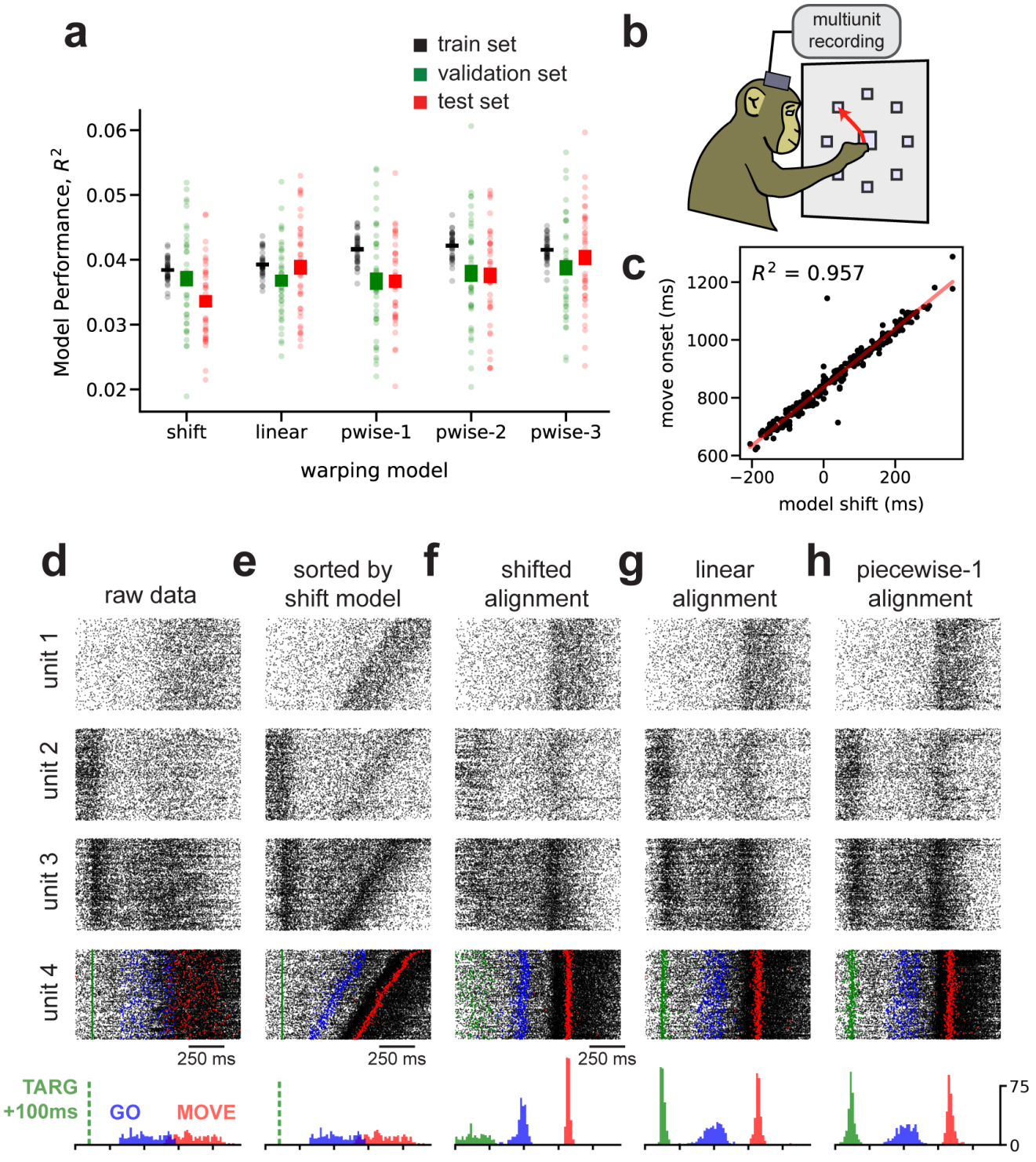

Figure S1. Related to Figure 4. Cross-validation and replication of movement onset detection in primate reaching experiment. (A) Nested cross-validation of primate reaching dynamics aligned to target onset (90° reaches). Solid boxes denote mean ± standard error for training (black), validation (green), and test (red) sets; dots show results for individual cross-validation runs ($n = 40$ randomized folds). (B-H) Replication of results in **Figure 4** with a new reach angle (135°). All figure panels are directly analogous to **Figure 4** in the main text and show comparable results.

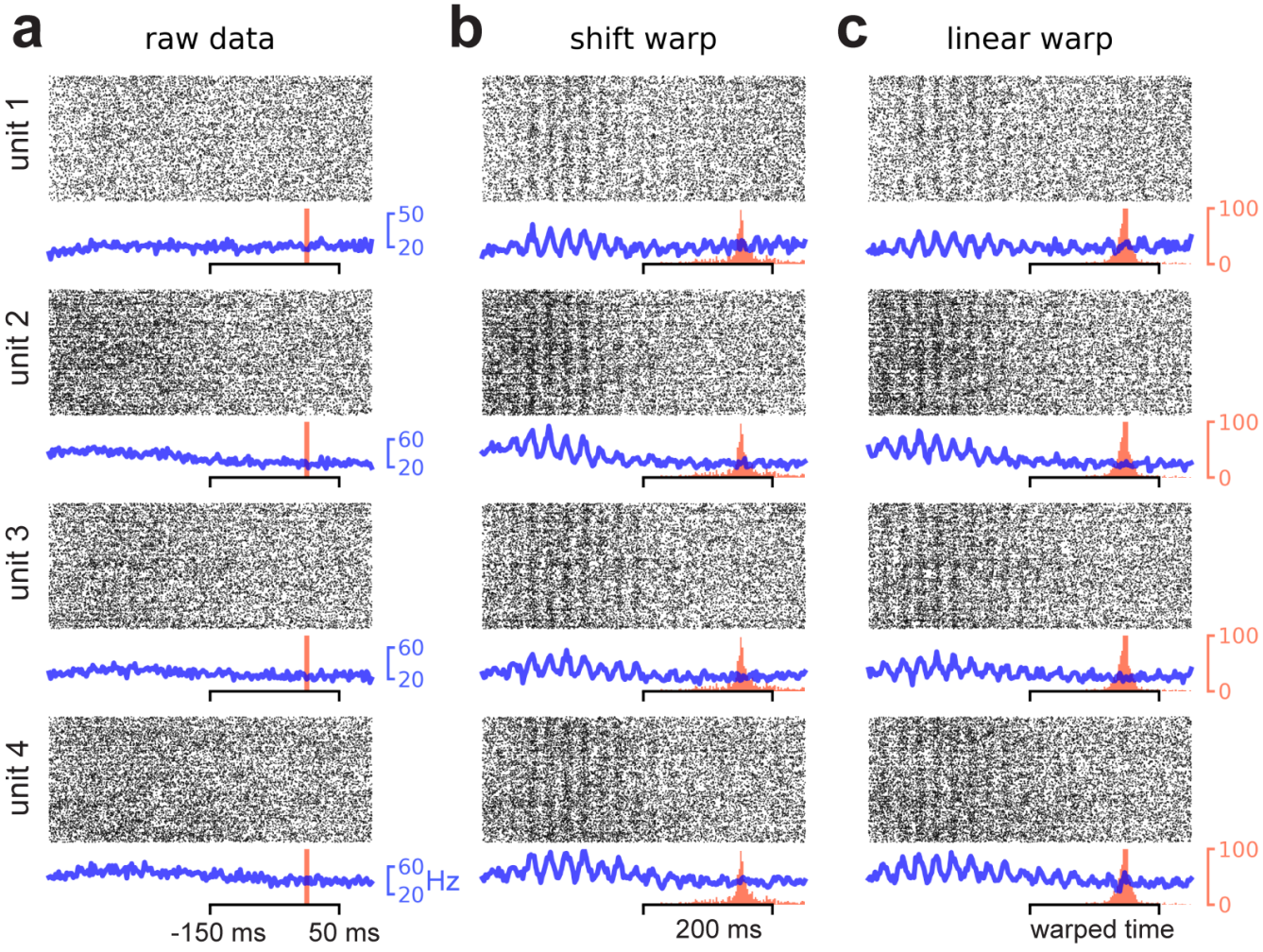

Figure S2. Related to Figure 5. Oscillations in premotor cortex uncovered in data from a second nonhuman primate. (A) Trial-by-time raster plots (black) and trial-averaged estimates of firing rate (blue) for four example multiunits. Red vertical line denotes the time that the go cue was delivered. (B-C) Same as panel A, except after spike times aligned by shift-only time warping (B) or linear time warping (C). Red histogram shows the distribution of go cue times after after the time warping transformation was applied. All four multiunits were held out during model fitting—the warping functions were fit to the remaining $N = 95$ units and applied to the held out multiunit to generate the displayed raster plots.

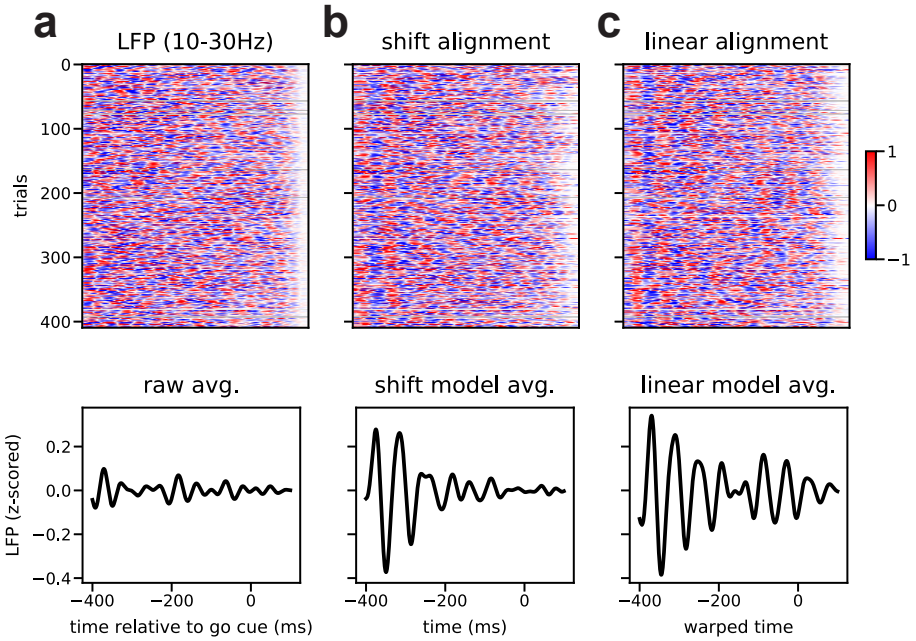

Figure S3. Related to Figure 5. Spike time oscillations in primate premotor cortex align with LFP. (A) Top, LFP signal on all trials. The signal was obtained by averaging over all $N = 96$ electrodes, z-scoring the signal within each trial, and then bandpass filtering (10-30 Hz; fifth-order Butterworth digital filter). Bottom, average LFP signal across trials. (B-C) Same as panel A, except after applying temporal alignments from a shift-only warping model (B) and a linear warping model (C). In both cases, time warping uncovered strong oscillations at ~18 Hz—the same frequency of spike-level oscillations identified in Fig 5. Importantly, the warping models were fit *only* to binned spike times, demonstrating that the model generalized well to new data stream with fundamentally distinct features. This suggests that the spike-level oscillations described in Fig 5 are time-locked with LFP oscillations, in agreement with prior work (Murthy and Fetz 1992; Sanes and Donoghue 1993; Reimer and Hatsopoulos 2010; Pandarinath et al. 2018). All data were taken from the same animal subject shown in Fig 5.

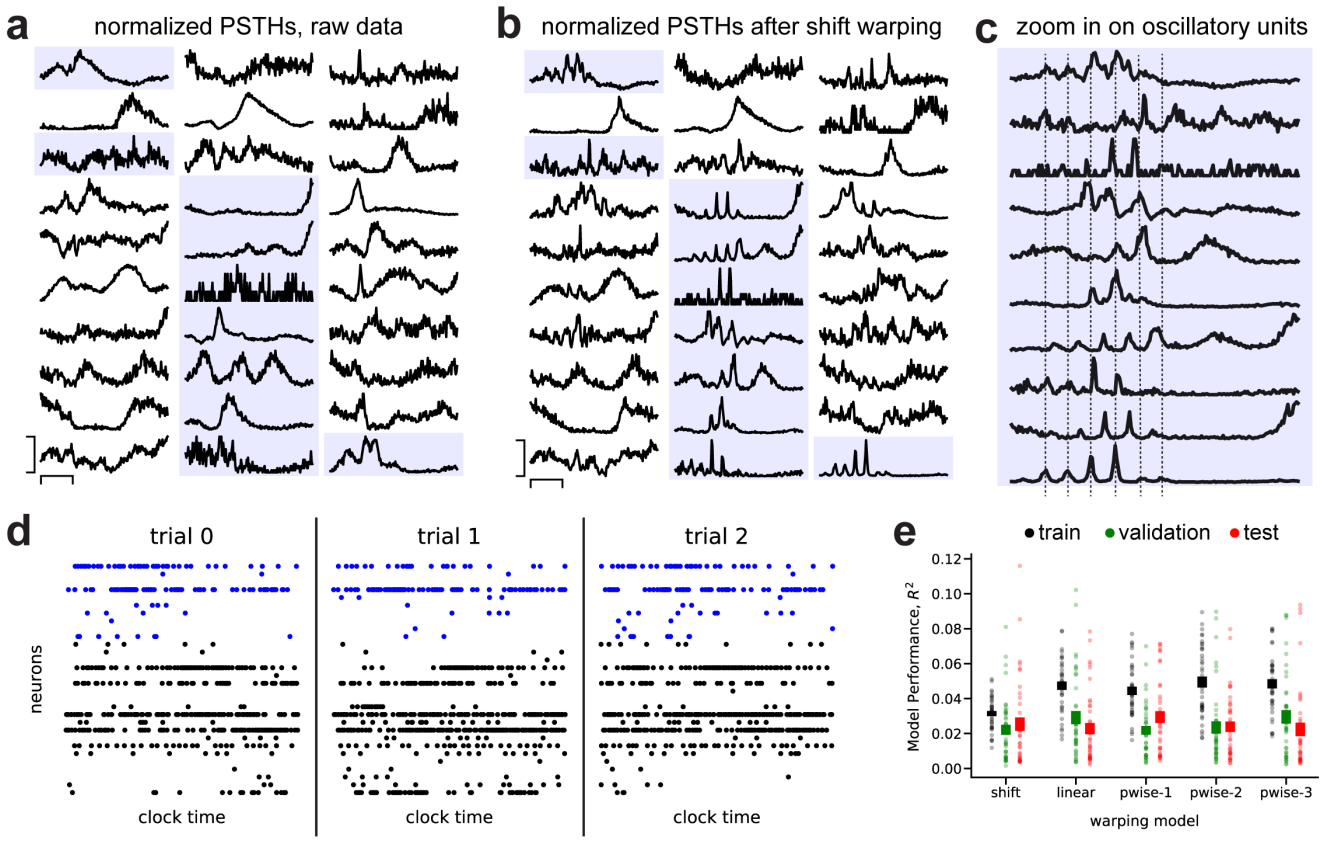

Figure S4. Related to Figure 6. Oscillations revealed in rat motor cortex are not phase-aligned across units, and not visible in population rasters. (A) Normalized peri-stimulus time histograms (PTSHs) of all $N = 30$ neurons, aligned to first lever press. PSTHs were normalized to range from zero (minimum firing rate) to one (maximum firing rate) with a bin size of 10 ms. Horizontal scale bar denotes 500 ms. Vertical scale bar denotes minimum to maximum firing rate for each neuron. Shadded blue backgrounds highlight example units with visible oscillations after time warping. (B) Same procedure as panel A, except PSTHs were computed on the aligned spike times of the shift-only warping model shown in **Fig. 6** in the main text. (C) Enlarged version of highlighted traces in panel B. Dashed black lines denote the time of firing rate peaks in the bottom unit (which displays particularly strong oscillations). Note that many units oscillate at different phases and also at different times during the behavior. Thus, averaging firing rates across neurons does not reveal oscillatory structure. (D) Three example trials visualized as a population raster plot. Blue dots denotes spikes from oscillatory neurons highlighted in panels A-C. Each raster shows the full two seconds of spiking activity. (E) Results of nested-cross-validation on dataset shown in **Figure 6**. Solid boxes denote mean ± standard error for training (black), validation (green), and test (red) sets; dots show results for individual cross-validation runs ($n = 40$ randomized folds).

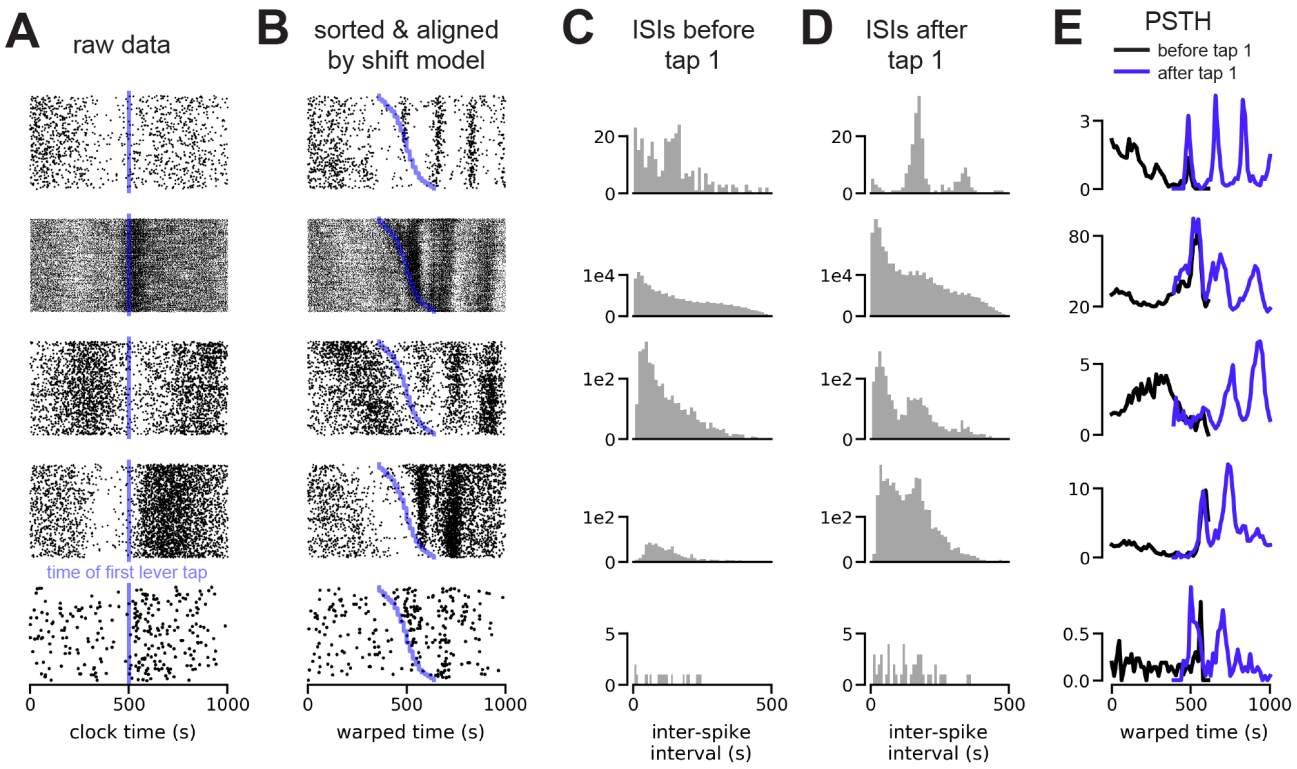

Figure S5. Related to Figure 6. Five representative isolated units exhibiting stronger spike time oscillations following the first lever press. (A) Raw spiking activity in a 1 second window around the first lever press. Vertical blue line denotes the time of the first lever press (manual alignment point). (B) Model-aligned spiking activity by shift-only warping, with trials sorted by the direction and magnitude of the learned shift. Blue line denotes the time of the first lever press on each trial. (C) Inter-spike interval (ISI) distributions during the 500 ms preceding the first lever press. (D) ISI distributions during the 500 ms following the first lever press. Note increased peak around ~150 ms, corresponding to increased oscillations at ~7 Hz. (E) Trial-averaged PSTHs for model-aligned spike times. Black lines denote PSTHs computed from spikes preceding the first lever press, while blue lines denote PSTHs computed from spikes following the first lever press. Note increased oscillatory dynamics following the lever press.

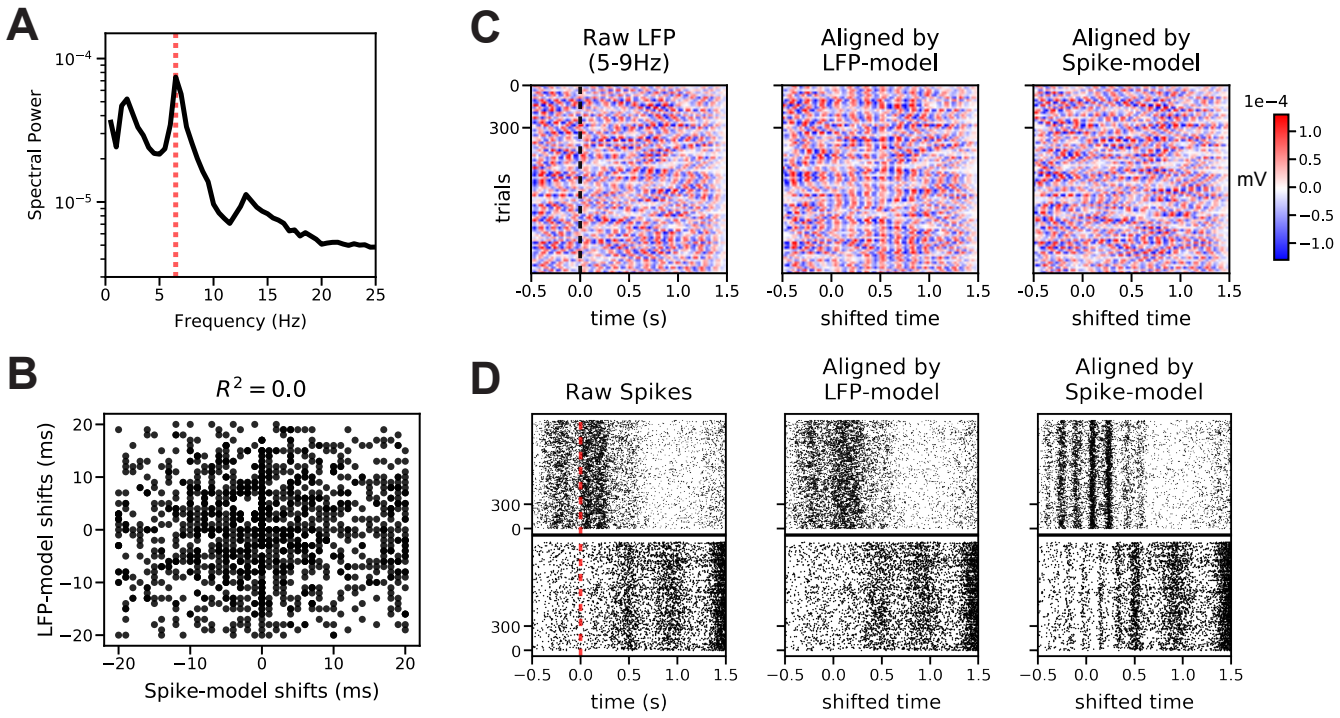

Figure S6. Related to Figure 6. LFP does not correlate with spike-level oscillations in rat motor cortex. The LFP signal was highly correlated across all electrodes and thus averaged across electrodes before analysis. (A) Trial-averaged periodogram of the LFP signal. Dashed red line denotes 6.5Hz, illustrating a peak in the LFP spectrum that is similar to the frequency of spike-level oscillations in **Fig 6**. (B) One shift-only time warping model was fit to bandpassed-filtered LFP signals (LFP-model; fifth-order digital Butterworth, 5-9 Hz), and a second shift-only time warping model was fit to binned spike trains (Spike-model; same as **Fig 6**). The scatterplot demonstrates the per-trial shift parameters learned by these models were not correlated, suggesting that the spike-level oscillations are not phase-locked to LFP. (C) Bandpassed LFP as raw data (left; dashed line denotes first lever press), and same data aligned by LFP-model (middle) and Spike-model (right) time warping models. LFP is not reliably aligned by the time warping model fit to spiking data. (D) Raster plots from two example neurons (top and bottom rows), showing raw spike times (left; dashed line denotes first lever press), aligned by LFP-model (middle), and aligned by Spike-model (right). Spike-level oscillations are not revealed by the time warping model fit to LFP.